

SUBSTORM CURRENTS: GROWTH PHASE AND ONSET

Richard L. Kaufmann

Department of Physics, University of New Hampshire, Durham

Abstract. Magnetic field models are used to study electric currents that flow during growth phases and onsets of magnetospheric substorms. Large cross-tail currents between altitudes of about 7 and 10 R_E are required near midnight during growth phase in order to produce the observed magnetic field perturbations at synchronous altitude. Considerations of the particle fluxes needed to carry growth phase currents showed that the required current can be carried by the drift of a particle population whose energy density is about 20 keV/cm³. This energy density frequently is present at synchronous altitude after injection events. However, the model calculations require establishment of the large currents beyond synchronous altitude during growth phase. No observations of substantial flux increases during growth phase within the region of interest could be found. As a partial explanation of this problem, we found that a modest increase in particle energy density can produce a substantial increase in cross-tail current. The increased currents carried by unaccelerated preexisting particles in the changing growth phase magnetic field can play a significant role in altering the magnetic field at synchronous altitude. This process involves a positive feedback effect, with preexisting particles carrying more cross-tail current as soon as any perturbation begins to stretch tail field lines. It is concluded that more extensive observations of the changes in particle fluxes and pitch angle distributions during growth phase are needed in the equatorial region near 8 R_E . Such observations also will help determine whether the energy of the plasma that is injected near synchronous altitude during substorms primarily is introduced slowly as fluxes build up during growth phase or primarily is introduced suddenly by the local conversion of magnetic field energy to particle energy at onset. In the first case, an injection event primarily would represent the inward motion of a population which already exists at substorm onset. In the latter case, strong impulsive acceleration would be an intrinsic part of the injection process. For our calculations, substorm onset is modeled by diverting current to the ionosphere in a wedge near midnight. It is found that field lines within the wedge collapse dramatically even if only a portion of the cross-tail current is diverted. At the same time, a satellite outside the current wedge sees field lines become more taillike. It is suggested that diversion of only the electron cross-tail current to the ionosphere is enough to initiate a substorm. Ion drift is reduced substantially within the wedge as field lines become more dipolar even if the ion energy density remains

large. Finally, it is noted that very strong drift shell splitting effects should be seen if cross-tail current is diverted only in a wedge near midnight.

Introduction

Currents in the extended magnetotail plasma sheet are estimated easily by considering the differences in B_x and B_y (solar magnetospheric coordinates) across the neutral sheet. For example, if $B_x = +20$ nT north of the neutral sheet and $B_x = -20$ nT south of the neutral sheet, then the net dawn to dusk sheet current density, integrated across the thickness of the current sheet, must be

$$K_y = 2B_x/\mu_0 \quad (1)$$

or numerically, $K_y = 32$ mA/m. Satellite measurements near and beyond 15 R_E show increases in B_x during the growth phase of a substorm [McPherron, 1972; Baker et al., 1981] indicating that K_y usually increases by about 10 mA/m during a moderate growth phase.

The much stronger (100 nT) magnetic field at synchronous altitude undergoes substantially larger changes during growth phases of many substorms. The growth phase usually is defined as the 15- to 60-min period preceding substorm onset during which large magnetic field and particle flux changes are seen at synchronous altitude and beyond [McPherron, 1972]. Substorm onset is defined as the time that large magnetic field and precipitating electron flux changes suddenly are detected by ground observers. For example, at ATS 6, which is located 10° from the magnetic equator, the field direction can change by several tens of degrees from nearly dipolar to a highly stretched configuration during growth phase. The magnitude of the magnetic field perturbation vector exceeds 50 nT for moderate or large substorms [Kokubun and McPherron, 1981]. This observation suggests, as frequently has been noted in the past [e.g., McPherron, 1972], that the largest currents and magnetic field energy changes take place in the inner tail (below about 10 R_E). The purpose of this work is to investigate the location, strength, and nature of electric currents that are needed to produce magnetic field perturbations seen near synchronous altitude during typical substorm growth phases and onsets. We begin by using a very simple two-dimensional magnetic field model in order to estimate approximate values for the currents to be used in the succeeding more realistic three-dimensional model. These models are able to define the regions of space to be studied experimentally in more detail during substorm growth phase.

We next consider how energetic particle fluxes and kinetic energy densities may change during growth phase in order to produce the required currents. The large current increase before

Copyright 1987 by the American Geophysical Union.

Paper number 6A8540.

0148-0227/87/006A-8540\$05.00

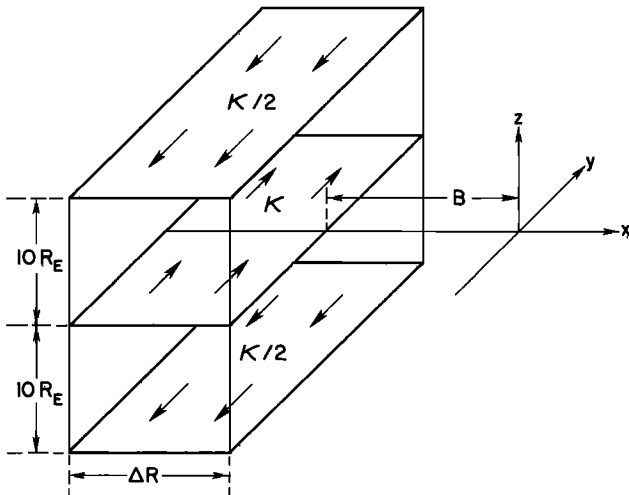


Fig. 1. Two-dimensional model of the magnetotail. A dipole placed at the origin and three sheet currents produce a taillike field configuration.

substorm onset may be associated with a significant input of energy into the magnetosphere during growth phase. In this event, much of the particle energy injected to and below synchronous altitude during substorms would build up gradually rather

than being transferred suddenly to the bulk of the substorm particles at onset.

Finally, electric current changes are investigated during substorm onset. It is found that a modest diversion of current to the ionosphere is sufficient to initiate a collapse of the inner magnetotail.

Growth Phase: Two-Dimensional Model

Figure 1 shows the simplest two-dimensional current model that can help to estimate the required sheet current density. A dipole is placed at the origin and a uniform infinitely thin current sheet with an inner edge at $x = -B$ and an outer edge at $x = -(B + \Delta R)$ flows from dawn to dusk in the equatorial plane. Return sheet currents are placed at $z = \pm 10 R_E$ to simulate the magnetopause. This two-dimensional model current system flows to infinity in the y direction, and therefore can provide an estimate of the magnetic field configuration only near midnight. Similar elementary models have been used in previous studies to show that the stretching of field lines near synchronous altitude can be produced by a reasonable increase in cross-tail currents at higher altitudes [McPherron, 1972; Lui, 1978; Sauvaud and Winckler, 1980]. We will introduce one of the much better standard three-dimensional magnetosphere models in a later section, but first

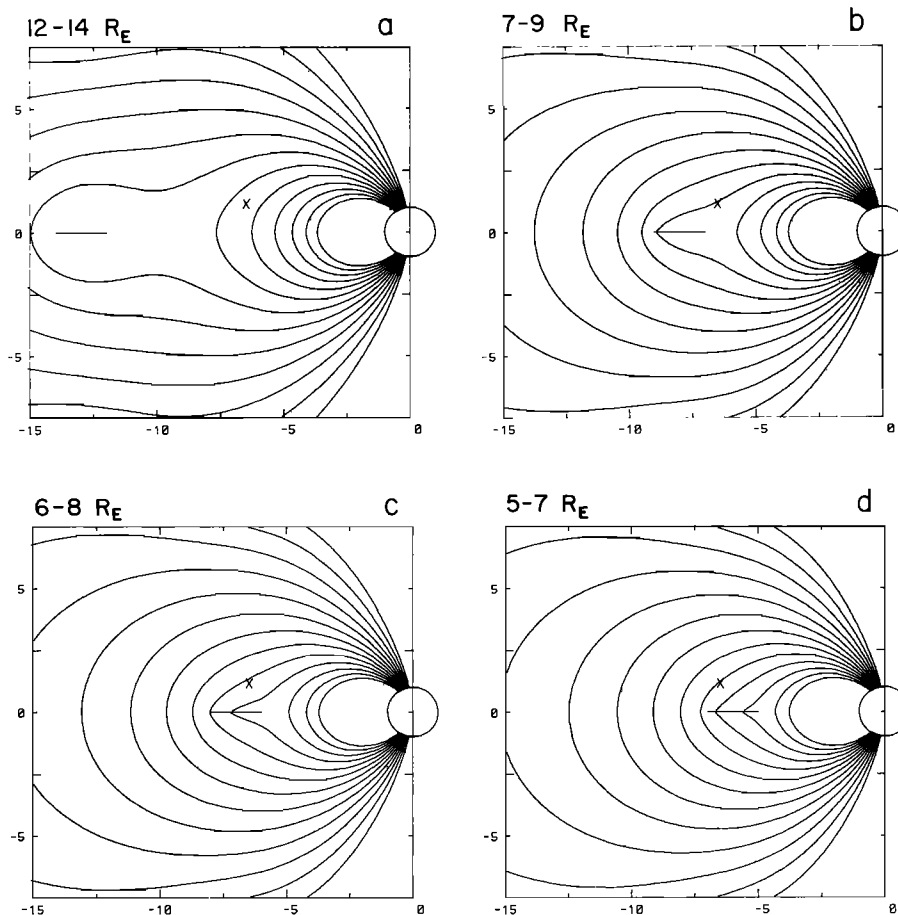


Fig. 2. Magnetic field lines in the two-dimensional model. The location of the current sheet is indicated by a straight line at the tail midplane, and by the label on each panel. The location of the ATS 6 satellite is indicated by a cross. The sheet current strength is $K_y = 300$ mA/m. Field lines are traced outward starting from the earth at 2° intervals from 57° to 81° magnetic latitudes.

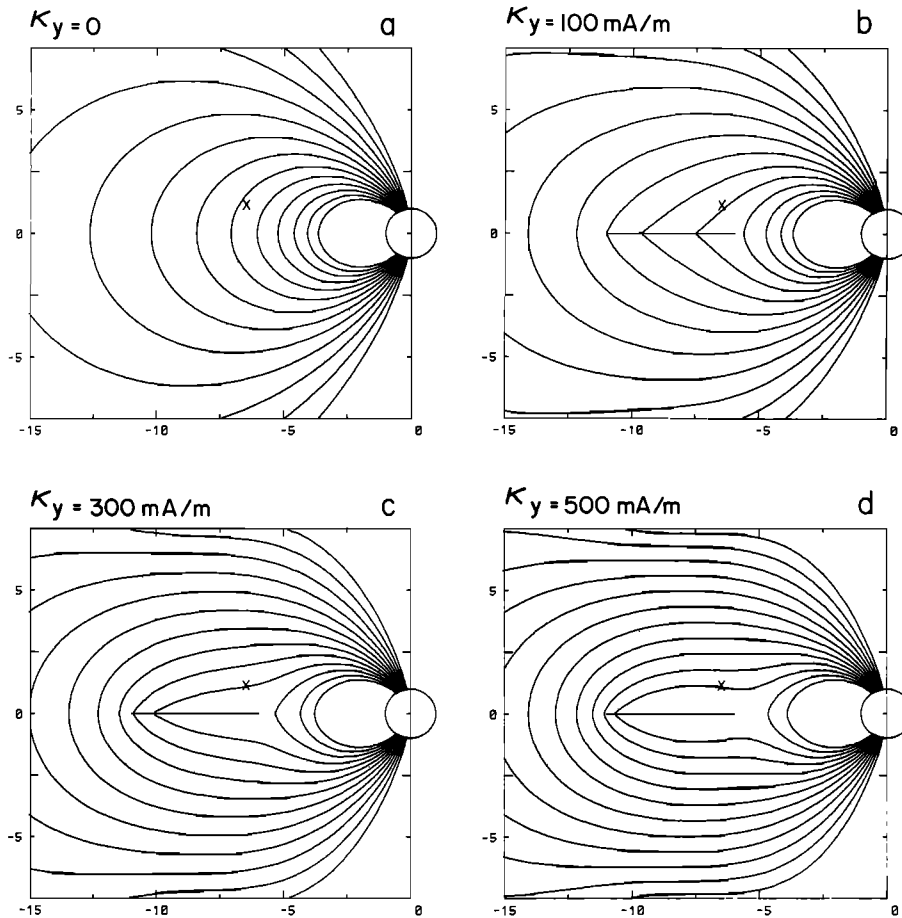


Fig. 3. Similar to Figure 2 except that the tail current sheet location is fixed and the strength varies.

will use the simple model to get a rough idea of the location and strength of tail currents that must be added to any quiet magnetosphere model in order to simulate growth phase.

As an initial step, we will see how moving the location of a cross-tail current sheet with fixed magnitude can affect magnetic field lines near synchronous orbit and at the ATS 6 geomagnetic latitude of 10° . The cross-tail sheet current strength is held at $\kappa_y = 300$ mA/m in Figure 2, and its extent is held at $\Delta R = 2 R_E$ while the inner edge is varied $5 < B < 12 R_E$. Adjacent field lines separated by 2° in latitude are traced out from the earth's surface in this figure, and extend from latitudes of 57° to 81° . It should be noted that the magnitude of κ_y is very large in comparison to typical cross-tail currents and current changes near and beyond $15 R_E$. Figure 2a shows that even when these very large currents are placed beyond $10 R_E$ in the tail they produce little distortion of field lines near ATS 6 (located at the cross in Figure 2a). Field lines at ATS 6 are strongly distorted in Figures 2b and 2c as the current sheet moves into synchronous orbit. The field at ATS 6 again becomes more dipolar as the current sheet moves below the satellite (Figure 2d).

Figure 3 gives an indication of field distortion and the motion of the satellite footprint as a current sheet, which now is fixed with edges at 6 and $11 R_E$, increases in strength. This fixed location is near the point at which

Figure 2 showed that currents are most effective in producing distortions near ATS 6. The extreme distortion from dipolar (Figure 3a) to taillike (Figure 3d) configuration at ATS 6 is associated with a motion of the latitude of the satellite footprint from 67° (the sixth lowest latitude line shown) to 61° (the third lowest latitude line shown).

Figure 4 summarizes the distortion in field direction (θ) and the change in field magnitude at ATS 6 when it is near midnight as a current sheet with a fixed radial extent, $\Delta R = 5 R_E$, is moved and changed in strength. For example, the upper panel shows that regardless of where in the equatorial plane a 30-mA/m current sheet is located, θ never is distorted by more than 6° . This indicates that the distortions observed at ATS 6, which frequently exceed $\Delta\theta = 20^\circ$ during moderate and large growth phases [Kokubun and McPherron, 1981], involve more than simply moving the typical cross-tail current sheet in to lower altitudes. Figure 4 shows that 20° and 40° distortions in the two-dimensional model require κ_y of approximately 100 mA/m and 200 mA/m if the plasma sheet inner edge is at $6 R_E$, and $\kappa_y = 170$ mA/m to $\kappa_y = 300$ mA/m if the inner edge is at $8 R_E$. The lower panel of Figure 4 shows that the field magnitude at ATS 6 generally decreases if the current sheet gets stronger when its inner edge is above the satellite altitude and generally increases as the current sheet strengthens if the inner edge is below the satellite.

The nature of field changes can be compared to

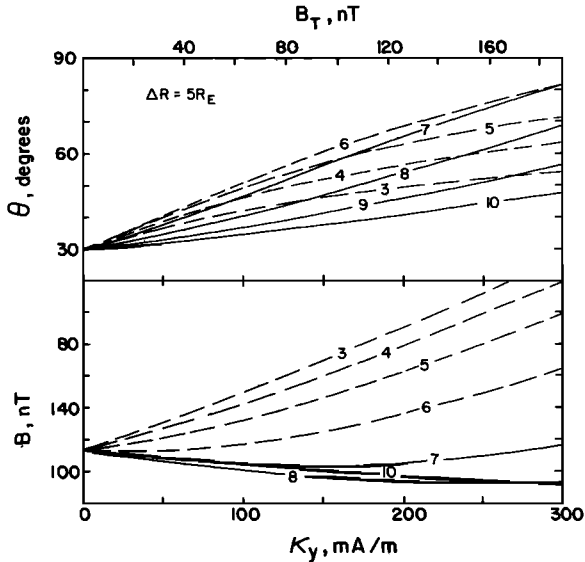


Fig. 4. Magnetic field strength and direction at the location of ATS 6 as a function of κ_y using the model in Figure 1. The angle θ is between the magnetic field direction and the z axis, so that $\theta = 30^\circ$ is dipolar and $\theta = 90^\circ$ is highly stretched. B is the total field strength and B_T is the maximum perturbation field that would be measured immediately above or below the center of the current sheet. Each curve is labeled by the radial distance to the current sheet inner edge in earth radii. All sheets extend outward a distance $\Delta R = 5 R_E$ from this inner edge.

experimental results from ATS 6. The satellite results are presented in the V, D, H coordinate system which is tied to the earth's dipole axis, with $H = B \cos \theta$. Kokubun and McPherron [1981] found that ΔH , the field recovery during a substorm expansion, is linearly related to H_0 and θ_0 , the values of H and θ at the end of growth phase. For example, a $\Delta H = 40$ -nT expansion onset is associated with $H_0 = 30$ nT, $\theta_0 = 76^\circ$. The corresponding values for $\Delta H = 0$ are $H_0 = 84$ nT, $\theta_0 = 44^\circ$. The differences between these two figures are $\Delta H = 54$ nT, $\Delta \theta = 32^\circ$, so that a 40-nT onset is associated with an approximately 54-nT growth phase during which θ changes by approximately 32° . In comparison, Figure 4 shows that $H = B \cos \theta$ changes by 55 nT when κ_y changes by 200 mA/m with $\Delta R = 5 R_E$ and the inner edge at $7 R_E$. At the same time, θ in Figure 4 changes by 35° , in surprisingly good agreement with observations considering the simplicity of the two-dimensional model.

Figure 5 more clearly shows the effects on θ and B of moving the plasma sheet inner edge when $30 \text{ mA/m} < \kappa_y < 500 \text{ mA/m}$ and $\Delta R = 2 R_E$ or $5 R_E$. The requirement for currents within about $2 R_E$ of the satellite in order to produce 20° to 40° changes in θ is evident. Substantial increases in field magnitude and a return of θ to its dipolar value require motion of the inner edge to low altitudes.

To summarize, even the very crude two-dimensional model allows us to draw two important conclusions:

1. It is not possible to simulate the tail stretching seen during even modest substorms with

reasonable equatorial sheet currents that are located only beyond $10 R_E$. The largest magnetic field perturbations seen before strong substorms require currents within about $2 R_E$ of the satellite.

2. The sheet current which must appear and disappear in this inner tail region during large substorms must be nearly an order of magnitude stronger than typical cross-tail currents which are seen at and beyond $15 R_E$.

These two conclusions will be shown to be required with a much better three-dimensional model in the next section. Some of the consequences of these results are discussed later.

Growth Phase: Three-Dimensional Model

All three-dimensional calculations in this work are based on the magnetosphere model developed by Beard [1979] and Beard et al. [1982]. This model provides a good global representation of the earth's magnetic field, and it contains a number of physically meaningful adjustable parameters. Since we primarily are interested in electric currents, Plate 1a shows the current density crossing the noon-midnight meridian plane. (Plate 1 can be found in the separate color section in this issue.) The cross-tail current was evaluated by numerically integrating

$$\oint \vec{B} \cdot d\vec{l} = \mu_0 \int \vec{J} \cdot d\vec{a} \quad (2)$$

around $1-R_E$ squares covering the area shown. Standard quiet time parameters were used for this plate (Table 1). The principal magnetotail current sheet is evident near $z = 0$ beyond about $x = -10 R_E$ over the nightside of the earth. The current flows from dusk to dawn in regions shaded by vertical black lines, and from dawn to dusk elsewhere. The total cross-tail plasma sheet current is about 20 mA/m or less with the parameters used in this plate.

The reversal of cross-tail current which appears beyond $|z| = 10 R_E$ in the distant tail

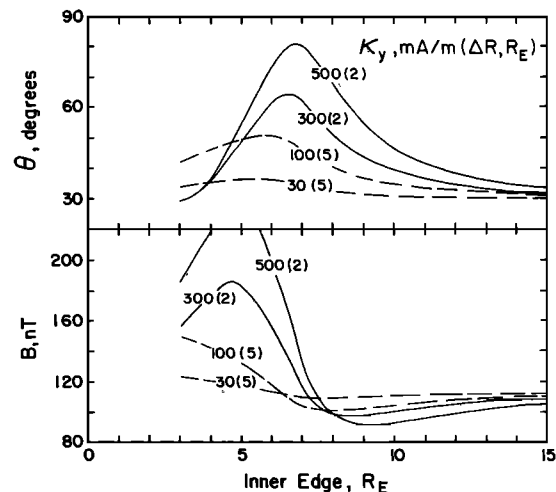


Fig. 5. Parameter definitions and the model used are as in Figure 4. Each curve is labeled by both the sheet current strength, κ_y , and its radial extent, ΔR . The location of the plasma sheet inner edge is varied.

TABLE 1. Parameters Used to Prepare Current Density Plots

Plate	b, R_E	s	n	z_0, R_E	RC, nT	B, R_E	$\Delta R, R_E$
1a	10	4	0.3	4	0	-	-
1b	10	4	0.3	4	20	-	-
2a	6	2.5	1	1	0	-	-
2b	10	4	0.3	4	0	6.6	3.5

Parameters are as follows: b is altitude of plasma sheet inner edge, s is inner edge shape parameter [Beard, 1979], n is exponent of tail field radial dependence, z_0 is plasma sheet half thickness, RC is ring current field depression at earth, B is inner edge of cross-tail line currents, and ΔR is radial extent of cross-tail line current region.

could represent part of the modeling of magnetopause currents. This effect also can be produced by the portion of cross-tail current which is attributed to individual particle drifts. Figure 1c of Wagner et al. [1979] illustrates this reversal of drift currents especially clearly. Propp and Beard [1984] used the model in Plate 1a to show that the adiabatic drift approximation provides a reasonable estimate of cross-tail current even for particles which follow complicated nonadiabatic orbits.

Currents near the earth are not correctly reproduced by the model because it, in common with many other models, uses a spherical harmonic expansion to represent the magnetic field in this low-altitude region. The integral in (2) is zero for fields generated by spherical harmonics. The weak currents that appear near the earth in Plate 1a are residual effects of that portion of the model used to fit tail magnetic field measurements rather than effects of the terms used to fit low-altitude measurements. Plate 1b shows that it is easy to add a model ring current, which will yield currents that at least are in the correct direction at low altitudes, without producing major distortions elsewhere. The ring current added to Plate 1b is that proposed by Tsyganenko and Usmanov [1982] using a radius of $4 R_E$ and a strength of $Dst = -20$ nT at the earth (Table 1). Since this addition does little to change the field direction at the ATS 6 satellite location, it has been omitted from other figures.

Changing Parameters

The simple two-dimensional model showed that we must introduce a thin current sheet approximately 10 times as strong as the quiet time currents shown in Plate 1, and that the inner edge of this new sheet must be placed near $x = -8 R_E$ in order to stretch the ATS 6 field line as observed during a large substorm growth phase. Plate 2a illustrates one of the many parameter changes that was attempted (Table 1). (Plate 2 can be found in the separate color section in this issue.) In this case, the plasma sheet characteristic thickness was reduced from 4 to $1 R_E$, the inner edge of the strongest part of the current sheet was moved in to about $7 R_E$, and the shape of the inner edge of the current sheet and the rate of decay of currents in the tail were modified. However, we were unable to adjust parameters at the inner edge of the plasma sheet so that the field lines at ATS 6 became as stretched as

observed. The growth phase changes that are needed to model the observed magnetic field perturbation primarily involve the addition of very strong cross-tail currents to the inner edge of the normal current sheet shown in Plate 1. Although the model used was quite flexible in modeling many of the observed global changes in the magnetosphere, we were not able to introduce the necessary highly localized currents by varying the adjustable parameters.

Addition of Line Currents

In Plate 2b we have used all the same parameters as in Plate 1a except that 14 cross-tail line currents were added between $x = -6.5$ and $x = -10 R_E$. Half of these currents were closed in semicircles near the northern and half near the southern magnetopause. The location and magnitude of each current loop are specified independently so they easily can be merged smoothly to the inner edge of the plasma sheet. The particular locations and strengths used in Plate 2b were selected to approximate the uniform sheet current in Figures 2-5 so that results of the three-dimensional model can be compared more readily with results from the earlier two-dimensional model. The average current strength between -6.5 and $-10 R_E$ is 200 mA/m in Plate 2b.

It is unfortunate that we could not obtain a reasonable fit to measurements at synchronous altitude during substorm growth phase without adding these line current loops. The infinitely thin loops and the infinitely thin current sheets used previously both are physically unrealistic since magnetic fields become arbitrarily large as one gets close enough to such a structure. The closure of currents in a sharply defined sheet on the magnetopause also is unrealistic, so that the basic well-behaved global magnetic field model can no longer be used throughout the magnetosphere. For this reason, we will only use the model with line currents to study field lines that pass near synchronous altitude. These problems associated with the use of line currents has been recognized in many previous magnetosphere models [Olson, 1974].

Figure 6b shows projections on the x - z plane of a group of field lines that cross the equator $2 R_E$ from the noon-midnight meridian plane (at $y = 2 R_E$) for the model field in Plate 2b. The distortion at the ATS 6 location is similar to that seen in Figure 2b, and is typical of the distortions seen during the growth phases of

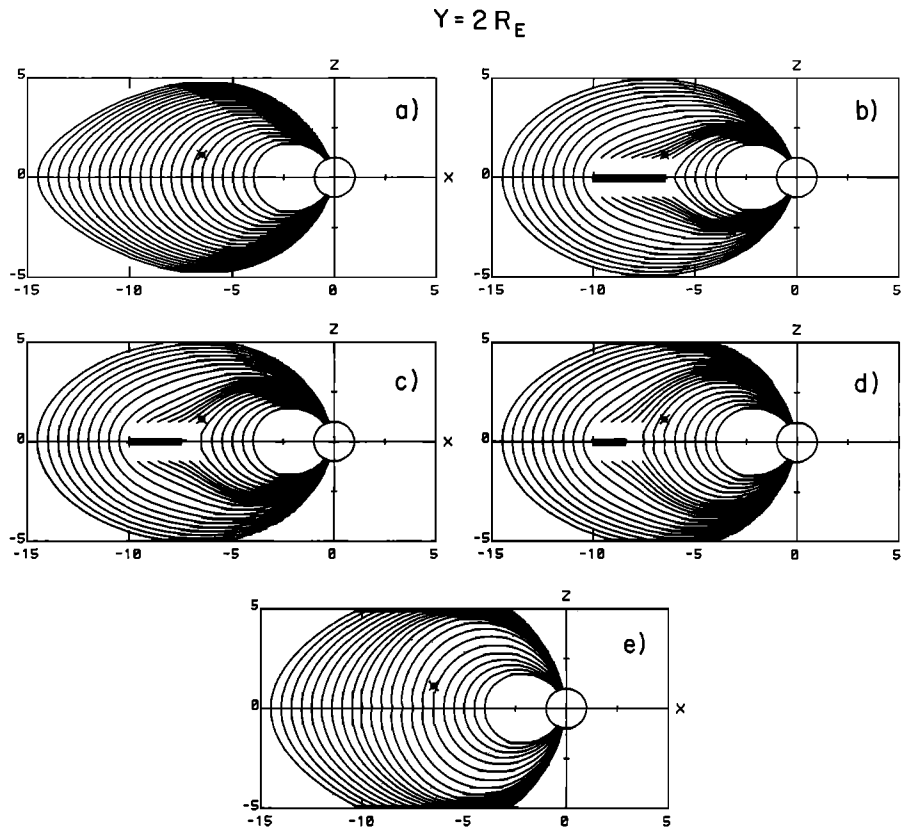


Fig. 6. Effects of diverting the cross-tail currents, as seen by a satellite located at $y = 2 R_E$. (a) Field lines in quiet magnetosphere model. These lines were traced down from the equator to the earth, starting at $0.5 R_E$ intervals in x . (b) Fourteen dusk cross-tail current loops have been added between $x = -6.5$ and $x = -10 R_E$. The loops are closed on the magnetopause, and each carries 3.2×10^5 A. (c) The innermost $1 R_E$ ($-6.5 R_E > x > -7.5 R_E$) of cross-tail current has been diverted to the ionosphere by adding four field-aligned current loops (two in each hemisphere). The added loops extend from $y = -4 R_E$ to $y = 4 R_E$ at the equator and carry dusk to dawn current in this region to approximately cancel the effects of the original cross-tail currents. The new loops are closed in the ionosphere by tracing along quiet time field lines. (d) The innermost $2 R_E$ of cross-tail current has been diverted. (e) All cross-tail currents are diverted.

moderate substorms. Tracing of field lines that would pass very close to the line currents was started at $z = 1 R_E$ in order to avoid the region in which fields are unrealistic. All other field lines start at $z = 0$, and are spaced at $0.5 R_E$ increments along the x axis.

Current Carriers

Apparent Problems

The large currents shown in Plate 2b must be carried by a population of energetic particles during the growth phase of a substorm. We concluded that these particles probably are located near $8 R_E$ and that it at least is necessary to locate a substantial fraction below $10 R_E$.

There are two general processes that could lead to the required large cross-tail currents during growth phase. Either the energy density of charged particles near $8 R_E$ builds up (by injection of new particles or acceleration of existing particles), or those particles that

already are present start to carry more cross-tail current without any significant energy change. It is likely that both processes are important.

Synchronous altitude ion and electron data have been studied for many years [DeForest and McIlwain, 1971] and consistently have shown exactly the opposite substorm-associated changes from those one initially might expect from a consideration of magnetic fields and the required electric currents. Particle fluxes at synchronous altitude usually are lowest during the growth phase of a substorm. However, this is the time that the magnetic field becomes most taillike, indicating the presence of the strongest cross-tail currents somewhere in the magnetotail. Only minor effects are seen at the ground during growth phase [Nishida and Kamide, 1983].

Almost immediately at substorm onset, as determined by arrays of ground magnetograms, a synchronous altitude satellite which happens to be located near midnight sees a large increase in energetic electron and ion fluxes (injection event) so that now there are plenty of particles to carry cross-tail current. However, at this

TABLE 2. Plasma Parameters Used to Generate Table 3

Location	B_x , nT	B_z , nT	B, nT	$P_{\parallel} = P_{\perp}$, nPa
a	0	20	20	2
b	20	20	28	2
c	20	20	28	0
d	0	100	100	0
e	0	80	80	2

The five locations a-e are shown in Figure 7a.

instant the magnetic field becomes dipolar, indicating that cross-tail currents are not needed to account for synchronous altitude magnetometer data [Kokubun and McPherron, 1981].

Higher-altitude data which have been reported to date also do not appear to show the required current carriers. The tail plasma sheet becomes thinner and its energy density does not increase dramatically during growth phase. This suggests that there are fewer particles present to carry cross-tail current just when magnetometer data suggest that the strongest currents flow. The plasma sheet then expands after substorm onset so that more particles are present to carry current, at the same time that electric currents appear to decrease and field lines become more dipolar [Baker, 1984; Fairfield, 1984; Hones, 1984].

Missing Particles?

One possibility during growth phase is that high particle fluxes and an intense current sheet form in a very localized region at the inner edge of the plasma sheet, as shown in Plate 2b. If the current is carried by newly injected or newly accelerated particles, we would expect to see particle fluxes build up at $8 R_E$ during growth phase as the magnetic field is becoming taillike at synchronous altitude. In this scenario, the injection events primarily would involve the earthward motion of this preexisting energetic population rather than primarily a sudden acceleration process.

There do not appear to be any reported observations of a slow buildup of large particle fluxes during substorm growth phases. Such observations would be difficult to make with satellites whose orbits extend well above $10 R_E$ since such satellites sweep rapidly through the region of interest ($6.5 R_E$ to $10 R_E$). The flux dynamics on such satellites often are dominated by entering and leaving the plasma sheet as it expands and contracts rather than effects of the slow earthward expansion and intensification of the plasma sheet. A satellite near the equator with perigee near $6 R_E$ and apogee near $10 R_E$ would be well positioned to detect a substorm flux increase if it exists. In view of the great variability that is seen in magnetospheric phenomena it is hard to believe that fluxes always build up to high values during growth phase near $8 R_E$ and never do so at synchronous altitude during growth phase. Nevertheless, we know of no observations of such flux increases at $6.6 R_E$ during growth phase.

The Active Magnetospheric Particle Tracer Explorers (AMPTE) CCE satellite has an elliptical

orbit with an apogee of $9 R_E$, so it may remain in the region of interest throughout a substorm growth phase. The SCATHA satellite surveyed the region from below synchronous altitude to an apogee of $7.8 R_E$ (L values up to 8.3) and was near the equator, so it may be able to detect flux increases. Although we know of no detailed particle studies that investigated changes during growth phase, a survey of average particle fluxes was carried out by Mullen and Gussenhoven [1983]. This survey showed that the average energy density of 100-eV to 400-keV particles ranged from 17 keV/cm³ at 8.0 to $8.5 R_E$ to 27 keV/cm³ at 5.5 to $6.0 R_E$ for Kp = 2 and 3. The corresponding energy densities were 17 keV/cm³ and 38 keV/cm³ in these altitude ranges for Kp = 4 and 5. A number of much earlier studies also have emphasized the high energy densities seen in the inner plasma sheet [e.g., Schield and Frank, 1970]. However, the studies to date do not appear to have resolved the question of whether the increased current near $8 R_E$ primarily is carried by an increase in particle energy density (injection or acceleration) or primarily is carried by the unaccelerated preexisting particles which begin to drift faster and therefore to carry more cross-tail current. Details of such a potential current source are discussed in the next section.

Numerical Estimates

The purpose of this section is to provide estimates of the contributions that those particle flux and magnetic field changes which are observed during growth phase make to changes in cross-tail current. All numerical work is based on the plasma parameters in Table 2. The entries in Table 2 simply are estimates for a typical inner plasma sheet. They are not based on self-consistent calculations, so that drift of these particles in the model magnetic field will not generate the current patterns in Plate 1 or Plate 2. Table 2 is used only to help determine which particle drift terms are likely to be most important in various parts of the plasma sheet, and to make rough estimates of the particle fluxes that can be expected to carry growth phase cross-tail currents.

The relatively large value $B_z = 20$ nT was used throughout what we have called the "neutral sheet" (equatorial region) since we are interested only in altitudes of about $10 R_E$ and less. This relatively large minimum field also makes a discussion of gradient and curvature drifts meaningful even at the equator. Orbits are very complex so that the adiabatic drift approximations lose their meaning farther out in the tail where the field more nearly approximates a true neutral sheet [Speiser, 1965, 1967; Wagner et al., 1979; Propp and Beard, 1984]. A plasma pressure of $P_{\parallel} = P_{\perp} = 2 \times 10^{-9}$ Pa was used in Table 2, corresponding to the particle kinetic energy density $W = (3/2) P = 20$ keV/cm³ discussed previously with regard to SCATHA measurements [Mullen and Gussenhoven, 1983].

Gradient drift current. Electric currents near synchronous orbit usually can be attributed to three effects: gradient drift, curvature drift, and magnetization or diamagnetic current. The current associated with drift in a magnetic field gradient can be expressed as

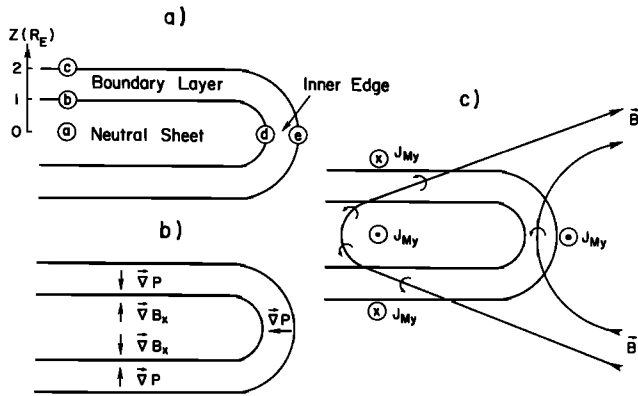


Fig. 7. (a) Locations in the plasma sheet that correspond to plasma parameters listed in Table 2. (b) Directions of principal magnetic field and plasma pressure gradients. (c) Magnetic field lines and positive ion orbits in the plasma sheet. These orbits, when combined with gradient information from Figure 7b, give the direction of cross-tail magnetization currents.

$$\vec{J}_G = P_{\perp} \frac{\vec{B} \times \vec{\nabla} B}{B^3} \quad (3)$$

$$J_{Gy} = \frac{P_{\perp}}{B^3} \left(B_z \frac{\partial B}{\partial x} - B_x \frac{\partial B}{\partial z} \right) \quad (4)$$

where the perpendicular pressure is related to the mean perpendicular particle energy and to the particle density by $P_{\perp} = n \langle E_{\perp} \rangle$. The strongest currents and largest gradients in the inner plasma sheet are expected to be detected at the plasma sheet inner edge, near the neutral sheet, or in the plasma sheet boundary layer (Figure 7a and 7b).

Table 3 summarizes the resulting electric currents. Gradient drift currents are relatively weak in all regions. Only the first term in (4) was retained at the inner edge of the plasma sheet. In the neutral sheet, the second term in (4) gives $\kappa_{Gy} = -30$ mA/m with the parameters in Table 2. However, if $\partial B_z / \partial x$ is as large as 5 nT/R_E, the first term will completely cancel this component. We estimated $\kappa_{Gy} = -15 \pm 15$ mA/m in Table 3. The parameters in Table 2 give no gradient current in the plasma sheet boundary layer. If $\partial B / \partial z$ is 2 nT/R_E, a current of -10 mA/m will flow, and if $\partial B / \partial x$ is 5 nT/R_E, a current of +10 mA/m will flow. We have estimated a current of 0 ± 10 mA/m in Table 3.

Curvature drift current. The electric current associated with drift due to curvature of a magnetic field line can be written

$$\vec{J}_R = P_{\parallel} \frac{\vec{R}_c \times \vec{B}}{R_c^2 B^2} \quad (5)$$

where $P_{\parallel} = 2 n \langle E_{\parallel} \rangle$ is the parallel pressure, and R_c is the radius of curvature of the magnetic field line. The curvature drift current is relatively strong (Table 3) and flows from dawn to dusk everywhere. As a result, curvature drift is an obvious candidate to explain field line stretching during growth phase. In preparing Table 3, we have assumed the field line radius of curvature is $2 R_E$ in all regions. It is important to note that the curvature current increases as R_c or B decreases, so that this current increases if P_{\parallel} or the particle energy density remains relatively constant and the magnetic field becomes more taillike.

Magnetization current. The magnetization or diamagnetic current can be written

$$\vec{J}_M = -\vec{\nabla} \times (P_{\perp} \frac{\vec{B}}{B^2}) \quad (6)$$

$$J_{My} = \frac{\partial}{\partial x} \left(\frac{P_{\perp} B_z}{B^2} \right) - \frac{\partial}{\partial z} \left(\frac{P_{\perp} B_x}{B^2} \right) \quad (7)$$

Figure 7c shows the source of these currents. At the inner edge and boundary layer of the plasma sheet, J_{My} is produced primarily by the diamagnetic effect of the pressure gradient. Positive particles move in the directions shown, and this gyromotion produces a net current in the regions in which particle densities change. The magnetization current at the neutral sheet is produced by the reversal of B_x and the resulting reversal of cyclotron motion rather than by a change in particle density. The first term in (7) dominates at the inner edge while the second term dominates in the neutral sheet and boundary layer. The small gradients discussed in the section on gradient drift current have been included in Table 3 to account for the smaller term in (7) for each region. Note that the net cross-tail magnetization current across the entire plasma sheet thickness (neutral sheet plus boundary layer) is small. Plasma pressure is assumed to drop to nearly zero beyond the boundary, so that almost all plasma is confined to the plasma sheet.

TABLE 3. Individual Contributions of the Three Major Sheet Current Sources to Total Cross-Tail Current in Three Regions of the Plasma Sheet

Region	Gradient	Curvature	Magnetization	Total
Inner edge	+10	+10	-50	-30
Neutral sheet	-15	+80	-130	-65
Boundary layer	+10	+40	+110	+150

Units are milliamperes per meter. Positive currents flow from dawn to dusk. Equations (3) to (7) were used with the assumptions in Table 2. Each region is assumed to extend $1 R_E$ in the z direction on each side of the equatorial plane.

TABLE 4. Properties of Maxwellian Electron and Ion (H^+) Populations That Could Carry Enough Adiabatic Current to Produce the Tail Stretching Observed at Synchronous Altitude

W, keV	n, cm^{-3}	$f_e, \text{s}^3 \text{km}^{-6}$	$J_e, \text{cm}^{-2} \text{s}^{-1} \text{sr}^{-1} \text{keV}^{-1}$	$f_i, \text{s}^3 \text{km}^{-6}$	$J_i, \text{cm}^{-2} \text{s}^{-1} \text{sr}^{-1} \text{keV}^{-1}$
0.1	200	6E4	4E10	5E9	9E8
1	20	200	1E9	2E7	3E7
10	2	0.6	4E7	2E4	9E5
100	0.2	2E-3	1E6	2E2	3E4

A total energy density of 20 keV/cm^3 was used to prepare this table. W is Maxwellian characteristic energy, n is density, $f(v)$ is distribution function at $v = 0$, and $J(E)$ is differential flux at $E = W$.

Changing Drift Velocities

Changes in the trajectories of energetic particles are very likely to contribute to the changes in cross-tail current. As was noted before, a number of studies have shown that adiabatic particle motion produces concentrated dawn to dusk currents near the neutral sheet and more distributed dusk to dawn currents at lower altitudes or in the tail lobes. The study by Propp and Beard [1984] used the same three-dimensional field model as Plate 1a, and showed that adiabatic gradient and curvature drifts provided a good approximation to the total cross-tail current even when the particles are not adiabatic. This net cross-tail current is dependent on the rate at which B_z decreases as one moves out the magnetotail.

As the tail becomes more extended, each particle contributes more to cross-tail currents because the magnetic field curvature and gradient both increase. Therefore, a degree of positive feedback exists as the tail stretches during growth phase and as it collapses during a substorm. As an example, when the tail begins to collapse toward a dipolar shape: each particle drifts less in the more dipolar field, the cross-tail current from curvature drift is reduced near $z = 0$, this current reduction leads to a more dipolar field, and the original perturbation is reinforced. In this way, it is possible for cross-tail currents to decrease substantially during a substorm even if only a small fraction of the current is diverted to the ionosphere. The process is discussed in more detail in the section on substorm onset.

Growth Phase: Summary

Magnetic field measurements at synchronous orbit were compared with magnetic field models to show that currents of $\kappa_y = 100 \text{ mA/m}$ or larger must flow from dawn to dusk near $z = 0$ during the growth phase of major substorms. This represents an inward motion and a large intensification of the innermost plasma sheet cross-tail current during growth phase. The particles which carry this current have not been clearly identified. They must have an energy density of about 20 keV/cm^3 , which is comparable to the energy density that commonly is injected at synchronous altitude after substorm onset. As an example, DeForest and McIlwain [1971] show pressure changes of 1 nPa (1

$\times 10^{-8} \text{ dyn/cm}^2$) or more during substorms, primarily carried by kilovolt electrons, in their Figures 14, 15, and 20. An isotropic pressure of 2 nPa corresponds to an energy density of 20 keV/cm^3 . Table 4 lists particle fluxes that would be seen in several Maxwellian plasmas with 20-keV/cm^3 energy densities.

Model calculations show that the current should be strongest near $8 R_E$ for a moderate or large growth phase. If this current is carried by newly accelerated particles, then energy must be directly transferred to these particles during growth phase. The lack of large ground effects during growth phase suggests that any newly accelerated particles will have a nearly empty loss cone at this time. In this scenario, the energy that is stored in the perturbed magnetotail field would not be the primary source of energy for particles which precipitate into the ionosphere and produce the principal substorm effects (auroras, field-aligned currents, electrojets, and the magnetic field perturbations seen by ground observers). Instead, energy would accumulate or be "stored" directly as kinetic energy of plasma sheet particles. Even in this case, stored magnetic field energy could produce effects which are seen after substorm onset in the more distant tail. There also certainly is some acceleration, particularly of the highest-energy particles, by induced electric fields during tail collapse. These effects will be discussed quantitatively in a separate publication for the specific field model used here.

It also is expected that the existing unaccelerated particles will carry more cross-tail current near $z = 0$ as field lines become more taillike. The numerical estimates suggested that curvature drift current is likely to produce a significant increase in cross-tail current during growth phase. The curvature drift current increases near $z = 0$ if the field lines become more stretched (R_c decreases in (5)) even if the particle pressure (or energy density) and all particle and magnetic field gradients remain unchanged. The actual cross-tail current increase is likely to be produced by a combination of these processes. In this way, a relatively small increase in particle energy density can produce a substantial increase in cross-tail current. Current carried by the new or accelerated particles perturbs the magnetic field and produces a more taillike configuration. Existing unaccelerated trapped particles drift faster near

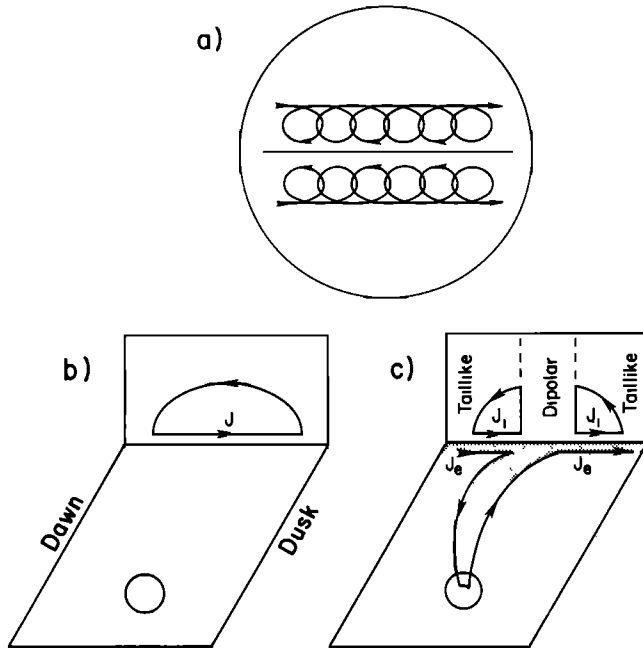


Fig. 8. (a) Sketches of the projection in the y - z plane of ion guiding center trajectories in a taillike magnetic field. (b) Net electric currents carried by ion and electron drift in a taillike field. (c) Ion and electron currents when electrons are diverted to the ionosphere only in a wedge-shaped region near midnight. The shaded region indicates the location of the plasma sheet.

$z = 0$ in this perturbed field, further enhancing cross-tail currents. It is suggested that a careful study of particle fluxes near $x = -8 R_E$, $z = 0$ could add a great deal to our understanding of the substorm growth phase.

Onset

Injection Boundaries

The most striking characteristic of substorms seen at synchronous altitude is the suddenness of plasma injection and the accompanying collapse or dipolarization of field lines. Figure 3 of Arnoldy and Moore [1983] shows an extreme example of a thin injection boundary. The entire electron flux change at all energies (the detector range extended from 0.06 keV to 23 keV) took place within 5 s, and the characteristic injection time (the interval between the 10% and 90% points in the flux change) was only about 2 s. Multiple satellite observations [Moore et al., 1981] have shown that injection boundaries move at about 100 km/s or less (corresponding to an electric field of 70 kV/ R_E or less), suggesting that the characteristic thickness of this injection front was not more than about 200 km. This characteristic length for electron flux changes is equal to the gyroradius of a 20-keV H^+ ion in a 100-nT field. If hot particle fluxes build up outside synchronous orbit before a substorm onset, this must at times take place in a region with an extremely sharp inner boundary. The idea that auroras represent one effect of a thin interface between two distinct plasmas has been suggested a

number of times in the past [e.g., Bryant, 1981; McIlwain, 1981; Kaufmann, 1984].

Injections often take place in multiple steps, with successively higher energy electrons each arriving suddenly at synchronous orbit [Nagai et al., 1983; Arnoldy and Moore, 1983]. This effect could be produced without requiring rapid local acceleration if tail collapse takes place in steps. During each step of tail collapse, the synchronous altitude satellite will be immersed in plasma that started farther out in the plasma sheet at onset. The observations therefore require the temperature of plasma which builds up during growth phase to increase with increasing altitude if this model is correct.

Current Diversion

One phenomenon that has appeared in the past to be very confusing is the continuity of currents which are diverted into the ionosphere at substorm onset [Kaufmann, 1984]. Conclusions from the preceding discussion of cross-tail current carriers help to clarify the situation. The current continuity problem is summarized as follows. In those cases in which field-aligned current carriers can be measured directly in the duskside region 1 current sector, they are found to be energetic or plasma sheet electrons. The current carriers in the dawnside region 1 sector are believed to be very low energy ionospheric electrons. However, energetic ions account for most of the energy density in the inner plasma sheet and in the newly injected substorm plasma [Mullen and Gussenhoven, 1983]. Therefore, ions carry much of the cross-tail current which must be stopped in order to produce the observed tail collapse or dipolarization, but ions are not diverted to the ionosphere as field-aligned currents.

Figure 8 schematically shows one way to explain this current continuity problem. The cross-tail current during growth phase is shown being produced by adiabatic drift of ion guiding centers in Figure 8a. Guiding centers of the positive ions shown in these sketches drift from dawn to dusk throughout the plasma sheet, corresponding to the gradient and curvature drifts in Table 3. The magnetization current corresponds to the net unbalanced dawn to dusk ion cyclotron motion at the plasma sheet boundaries and the net dusk to dawn cyclotron motion near the equator. Total current integrated throughout the plasma sheet is dawn to dusk in Figure 8a. Both ions and electrons contribute to these cross-tail currents, though only ion trajectories are shown. If particle orbits are adiabatic, the loss cones will be nearly empty and the increase in fluxes in the inner plasma sheet will not produce large ionospheric effects. Small ionospheric responses to growth phases have been detected by careful investigations of ground magnetograms [Nishida and Kamide, 1983]. An empty loss cone essentially decouples the magnetosphere from the ionosphere.

If some process begins to pitch angle scatter particles at $8 R_E$, the loss cones will fill and current will flow to the ionosphere. At very low scattering rates, where loss cones remain nearly empty, the relative rate of scattering of ions and electrons will determine the field-aligned current carriers. However, when scattering is rapid

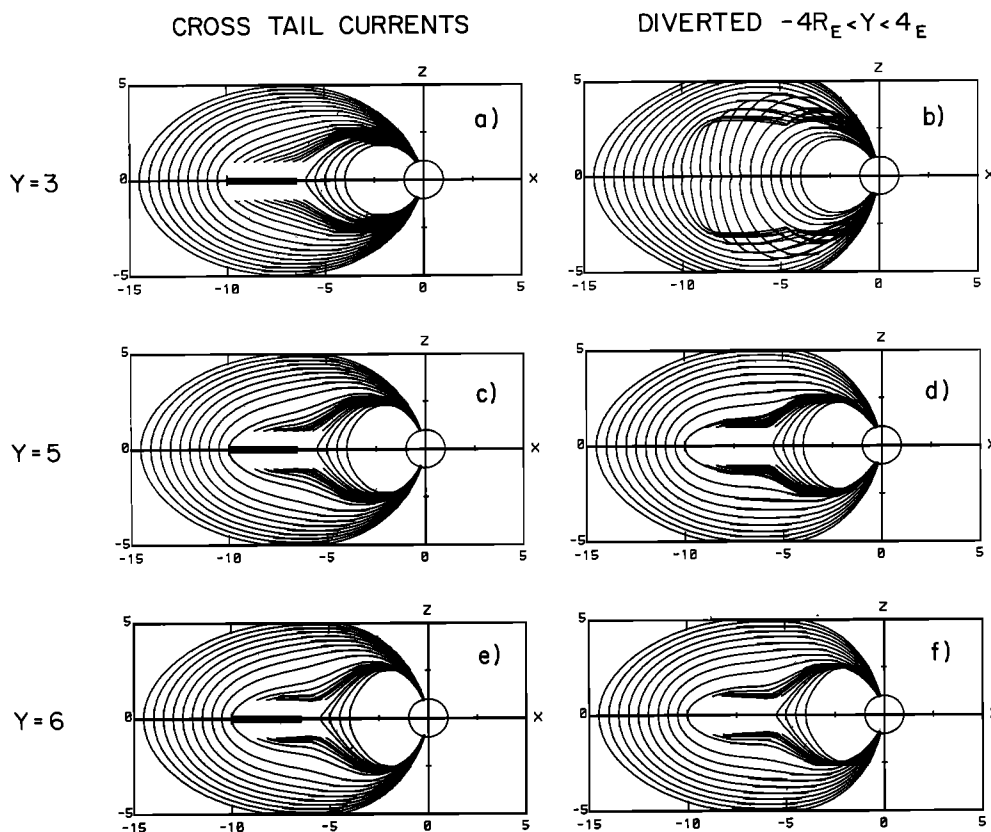


Fig. 9. Similar to Figures 6b and 6e, as seen by satellites located at $y = 3, 5,$ and $6 R_E$.

enough to maintain full loss cones, the electron field-aligned current will far exceed the ion field-aligned current because of the much higher electron velocities. Very low energy ionospheric electrons can flow to maintain charge neutrality as the ionosphere and magnetosphere become coupled. However, these ionospheric electrons have a very low energy density and therefore will not produce much cross-tail current even if their number density is high. As a result, the tail field lines will start to become more dipolar.

The above situation appears to be unstable. Curvature drift provides most of the net dawn to dusk current integrated across the plasma sheet (sum of neutral sheet and boundary layer currents in Table 3). If the field begins collapsing because electron current is diverted, the ion guiding centers will drift less in the more dipolar plasma sheet field, and this reduction in cross-tail current will accelerate the collapse. The ions do not go away and their cross-tail current is not diverted to the ionosphere, but the ion guiding centers simply stop drifting rapidly from dawn to dusk within the plasma sheet. The ion orbits remain similar to those shown in Figure 8a, but adjacent loops overlap much more in the dipolar field because guiding centers drift much less during each cyclotron period.

Figure 8b shows schematically the net current carried by electrons and ions when the field is taillike, as in Figure 8a. The net current flows from dawn to dusk in the plasma sheet. Current closure is illustrated schematically by the semicircle in Figure 8b. Actual current closure

could take place on or near the magnetopause or by the drift of ions and electrons on portions of their trajectories that are far from the plasma sheet. The figures in the works by Wagner et al. [1979] and Propp and Beard [1984] show net drift throughout complete particle trajectories in taillike magnetic field geometries. Since we primarily are interested in the localized currents that produce magnetic field changes near synchronous altitude, current closure will not be considered in detail in the present work.

Figure 8c shows the situation when electron current is diverted to the ionosphere, field lines become dipolar, and ion currents are greatly reduced at $z = 0$ only in a wedge near midnight. The shaded region is included to indicate that the plasma sheet inner edge moves earthward in the limited region of dipolar magnetic field lines. Atkinson [1983] discussed the evolution of such structures.

Model Calculations: Substorm Wedge

Figures 6 and 9 use the three-dimensional magnetosphere model to illustrate some of the interesting effects that take place when current is diverted to the ionosphere. Very large currents were used to prepare these figures in order to make the effects clearly visible. Figure 6b shows projections onto the x - z plane of field lines that reach the equator at $y = 2 R_E$ when a cross-tail current of 200 mA/m is flowing. The inner and outer boundaries of the current are at radial distances of 6.5 and 10 R_E . Figures 6c,

6d, and 6e show what a synchronous satellite would see at $y = 2 R_E$ if current in the wedge extending from $y = -4$ to $y = 4 R_E$ is diverted to the ionosphere. The field line at the satellite returns to approximately its quiet time configuration (Figure 6a) when the inner $1 R_E$ (Figure 6c) to $2 R_E$ (Figure 6d) of the cross-tail currents are diverted. If all added cross-tail currents are diverted to the ionosphere (Figure 6e), field lines near the satellite become substantially more dipolar than in the original quiet time model (Figure 6a).

A comparison of Figures 6b and 6e shows the dipolarization which is seen by a satellite at $y = 2 R_E$, when all cross-tail currents in the $-4 R_E < y < 4 R_E$ wedge are diverted to the ionosphere. Figure 9^e shows comparisons at the same two times as seen by satellites located at $y = 3, 5,$ and $6 R_E$. Very strong dipolarization is seen at $3 R_E$, which is inside but near the diversion point. The extremely strong field-aligned currents result in a spiraling of some field lines which get very close to the line currents in Figure 9b.

Field lines become more taillike rather than more dipolar as currents are diverted when viewed by satellites located outside the current wedge. For example, the field line crossing the equator at $x = -10 R_E$ is at a smaller $|z|$ when it reaches $x = -7 R_E$ in Figures 9d and 9f (with diversion) than in Figures 9c and 9e (before diversion). Such effects have been observed experimentally on synchronous satellites [Arnoldy and Moore, 1983].

Model Calculations: Field Line Mapping

Field lines in Figures 6 and 9 were traced from the equator to the earth so that they would cross the equator at the desired location. Figure 10 shows the footprints or intersection points with the earth's surface of field lines that start at $x = -6.5 R_E$ and a latitude of 10° . Point Q in each panel shows the footprint in the quiet magnetosphere model, and points a are the locations when the full cross-tail currents are flowing. The extremely strong (200 mA/m) currents used here move footprints of field lines starting at various y locations about 2° equatorward. Significant local time motion also is seen for field lines starting well away from midnight. When the innermost $1 R_E$ of cross-tail current is fully diverted to the ionosphere (points b), the footprints of field lines starting between $y = 0$ (midnight) and $y = 2 R_E$ (still well within the current diversion wedge) move back to near their quiet time locations. Diversion of the innermost $2 R_E$ (points c) or of all cross-tail current (points d) moves these footprints well poleward of their quiet time locations. Diversion of only the electron component of cross-tail current would produce less dramatic effects. Diversion in the wedge extending only out to $y = 4 R_E$ produces the opposite effect outside the current wedge. For example, field lines at $y = 6 R_E$ become more stretched, so that footprints move equatorward as more current is diverted to the ionosphere (points b, c, and d).

Pitch Angle Anisotropy

It has been known for many years [Kaufmann, 1963; Roederer, 1967] that particles with

different equatorial pitch angles move along substantially different shells as they drift from dipolar field lines near noon to taillike field lines near midnight. Figures 6 and 9 show that this same drift shell splitting effect is concentrated into a small sector of the nightside magnetosphere when current is diverted in a wedge. Particles with 0° equatorial pitch angles must drift along very different paths from particles with 90° equatorial pitch angles when moving between the stretched field lines at $y = 6$ and the dipolar lines at $y = 2$.

As an example of the expected effects, assume an isotropic Maxwellian distribution is present on stretched field lines and that this isotropic distribution has a radial gradient so that higher fluxes are present at lower altitudes. When these particles drift to dipolar field lines, they will develop $J(90^\circ) > J(0^\circ)$ due to drift shell splitting. The opposite anisotropy will develop if the radial gradient is opposite, with higher fluxes at higher altitudes, as might be present at the inner edge of the plasma sheet. A number of papers have studied drift effects in substorm electric and magnetic fields [Kivelson et al., 1980; Mauk and Meng, 1983] but we are not aware of any that have investigated the changes expected from the introduction of a wedge in which cross-tail currents are diverted. Smits et al. [1986] have presented evidence that current diversion can be very localized, forming a sharp boundary as in our model. Fennell et al. [1981] and Arnoldy and Moore [1983] have shown examples of rapidly changing pitch angle distributions, some of which may be influenced by shell splitting effects.

Conclusions and Summary

Location and Strength of Currents

Growth phase. Figure 11 summarizes the changes that are required during a substorm at the inner edge of the plasma sheet, where dipolar and stretched taillike field lines meet. Before a substorm growth phase begins, the plasma sheet currents either are weak or are located beyond a radial distance of about $10 R_E$ (Figure 11a). The field is dipolar and particle fluxes are low at synchronous altitude.

Model calculations showed that cross-tail currents which are much more intense than those that exist in the distant (beyond $15 R_E$) tail must develop between about 7 and $10 R_E$ during growth phase. This development represents the inward motion and intensification of the inner edge of the plasma sheet. It is these cross-tail currents that are responsible for the severe magnetic field perturbations which are seen at synchronous orbit before the onset of moderate and large substorms. Figure 11b shows a new region of strong currents in the inner plasma sheet, and a thinning and stretching of field lines to produce a taillike field at synchronous altitude. With regard to growth phase, we draw the following conclusions:

1. Better magnetic field models with adjustable shape parameters are required to accurately describe the important region at the inner edge of the plasma sheet where field lines change from dipolar to taillike. Stern [1986] presented preliminary results from a model that

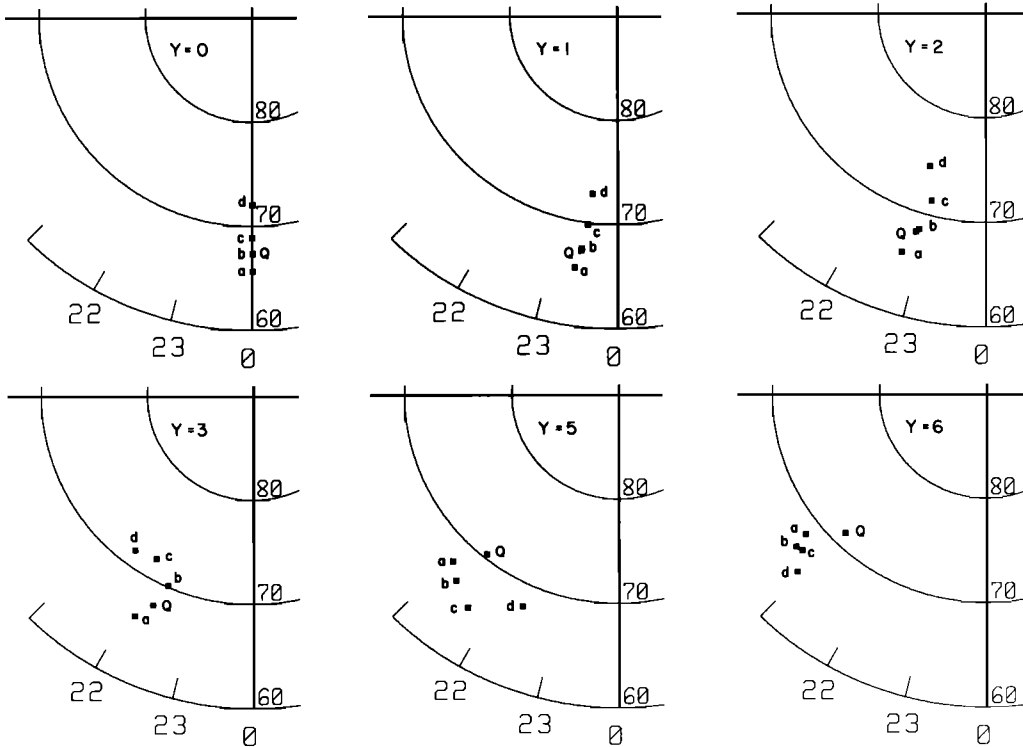


Fig. 10. Footprints of a satellite located at $x = -6.5 R_E$, a latitude of 10° , and at various distances from midnight. In each panel, the point labeled Q is the footprint for the quiet field model (Figure 6a and Plate 1). Points a, b, c, and d correspond to the models shown in Figures 6b, 6c, 6d, and 6e, respectively. All currents are diverted to the ionosphere at $y = \pm 4 R_E$.

may provide an adequate description of this region.

2. The particles which carry intense cross-tail currents during growth phase have not been identified clearly. The energy density and fluxes of these particles are estimated in Table

4, and are not unusually large. Table 4 is based on the assumption that a Maxwellian plasma with characteristic energy W and density n is present. The maximum of the distribution functions of H^+ ions and electrons (which occur at $v = 0$) and the maximum of the differential fluxes (which occur at

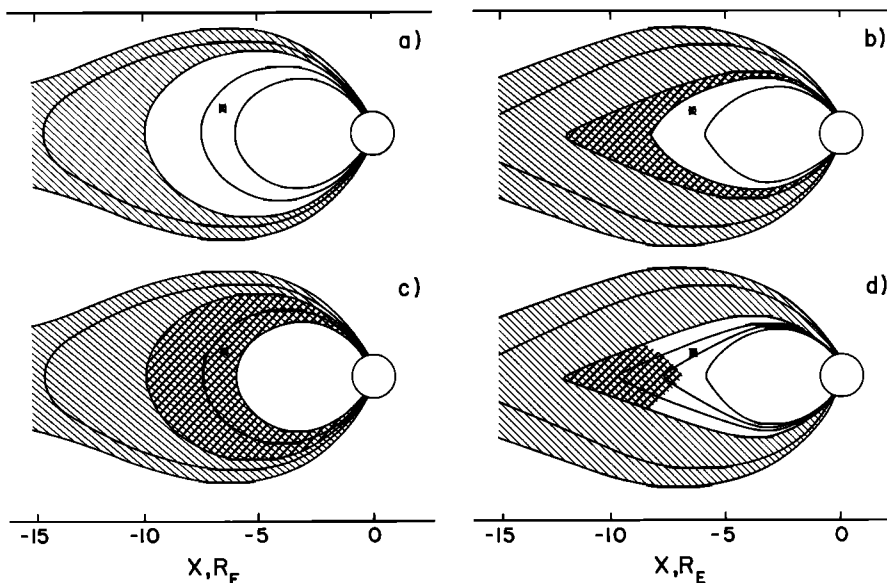


Fig. 11. Sketches of the magnetotail (a) before growth phase, (b) at the end of growth phase, (c) after onset of a substorm, and (d) at the end of growth phase with an equatorially trapped population.

E = W) are tabulated. Table 3 breaks down the expected currents according to source and region of space. The problem is that we have seen no experimental studies that have identified consistent increases in particle fluxes or changes in pitch angle distributions which should produce the large cross-tail current increases that are seen during growth phase.

3. It is pointed out that magnetic field line curvature drift is particularly important because the resulting cross-tail current increases when the magnetic field becomes more taillike even if there are no changes in particle fluxes or in particle or field gradients. This provides a positive feedback mechanism which enhances tail stretching once it has begun. Nevertheless, some unidentified flux change must take place during growth phase to initiate and sustain tail stretching. We have not been able to determine what fraction of the growth phase current increase is produced by an increase in particle energy density (through injection of new particles or acceleration of existing particles) and what fraction is produced by the increased drift of unaccelerated preexisting particles in the more stretched field. Experimental studies near $8 R_E$ at equatorial latitude should be able to identify the cause of growth phase current increases.

4. With regard to specific current carriers, any increase in particle fluxes during growth phase clearly can contribute to the current increase. An increase in field alignment of particle fluxes also will increase R_c and therefore curvature drift in the plasma sheet (5).

Gray and Lee [1982] and Propp and Beard [1984] showed that it is difficult to maintain highly anisotropic distribution functions in the magnetotail, but a small energy density of field-aligned or cigar-shaped electrons is regularly seen at synchronous altitude during growth phase [Baker et al., 1981]. It should be noted that the energy density of these electrons is far below that needed to carry the cross-tail currents which generate taillike field lines. The anisotropic growth phase energetic electrons are assumed to act like test particles which respond to global changes in the magnetic field rather than the current carriers which cause the field distortions [Paulikas and Blake, 1979].

Finally, if particles near $8 R_E$ are very strongly confined to the equator (equatorial pitch angle distributions strongly peaked at 90°), it is possible that they could have been missed by the satellites with highly elliptical orbits which have studied the inner plasma sheet. Very small energy densities of equatorially trapped plasma particles have been detected at lower altitudes [Olsen, 1981].

One attractive feature of this last mechanism is that it would simplify the explanation of why the ATS 6 satellite never appears to see significant particle flux increases during growth phase. Figure 11b shows that it becomes difficult to draw a sketch of highly stretched field lines in which the flux tube containing high particle fluxes both reaches the equator near or below $8 R_E$ (the region in which we concluded current must flow) and also is located beyond the 10° satellite latitude at $6.6 R_E$ (so that high fluxes will not be seen on ATS 6). For example, Figures 2 and 3 show that most of the highly stretched field lines

at ATS 6 pass through the current sheet in the two-dimensional model. We were unable to trace field lines to the equator in this region with the three-dimensional model. Fluxes at ATS 6 would be expected to increase during growth phase if the current sheet particles were isotropic or field-aligned and were on the same field line as ATS 6. Only equatorially trapped particles could exist on the same field line as ATS 6 without producing a large flux increase during growth phase (Figure 11d).

In general, the above points emphasize the importance of good pitch angle and flux measurements by a satellite that remains at a nearly fixed location between $R = 6.6$ and $10 R_E$ throughout substorm growth phase. As was noted previously, a careful study of data taken during growth phases by existing satellites may be sufficient to resolve some of the most important outstanding questions.

Substorm onset. Figure 11c shows the principal features near midnight associated with substorm onset:

1. Electric fields and the resulting $\vec{E} \times \vec{B}$ drift are very strong during a rapid injection event [Moore et al., 1981; Aggson et al., 1983; Smits et al., 1986], and therefore particles with all energies move together. This is in contrast to the varying inward motion according to particle energy and species that is expected if inward plasma sheet motion during growth phase is produced by an increase in the cross-tail electric field [Kivelson et al., 1980].

2. Portions of the inner edge of the plasma sheet appear to be extremely sharp at least during some injections. The well-known brightening of the equatorward quiet auroral arc at onset suggests that the substorm instability begins at this sharp plasma sheet inner edge.

3. Once the cross-tail current starts to decrease or the plasma sheet inner edge moves earthward, field lines become more dipolar. This change in geometry leads to a reduction of curvature drift near $z = 0$ thereby reinforcing the original perturbation. Most ions remain in the tail, but they carry much less cross-tail current near $z = 0$ in a dipolar field geometry than in a taillike field geometry.

Energy Sources

Although the model calculations cannot determine how particles gain energy, they may make an addition to the continuing discussion of the importance of driven and unloading processes during substorms.

Since large magnetic field perturbations are observed during growth phase, energy is stored in the magnetic field. The field magnitude usually does not change a great deal at the ATS 6 satellite location [Kokubun and McPherron, 1981]. Figure 5 shows that large magnitude changes, and therefore large changes in $B^2/2\mu_0$ near $6.6 R_E$, are expected if the current sheet inner edge moves earthward of the satellite. Dissipation of this stored energy could result in local acceleration of energetic particles, and it is certain that some adiabatic acceleration takes place when the tail collapses. However, it also is possible for this magnetic field energy to propagate away from the region near the cross-tail currents without

producing a great deal of energetic particle acceleration near and below synchronous altitude. For example, this energy could be dissipated in the acceleration of a plasmoid out the magnetotail [Hones, 1984].

The second possible energization mechanism involves the slow accumulation of kinetic energy by the cross-tail current carriers during growth phase. In this model only a small fraction of the particle acceleration would take place when the injection boundary moves inward at substorm onset. Since there is only a modest indication of substorm growth phase in ground observations [Nishida and Kamide, 1983] any fluxes of particles that build up in the inner plasma sheet must be stable during growth phase. The pitch angle distributions therefore would be expected to show an empty loss cone.

The most likely energy source in the slow acceleration model involves the increased flow of dawn to dusk current in the magnetotail dawn to dusk electric field. Stern [1980] pointed out that the rate at which energy is given to charged particles ($dW/dt = \mathbf{J} \cdot \mathbf{E}$) is much higher than is required to explain auroral and substorm processes. For example, if κ_V increases by 100 mA/m over a radial distance of only $2 R_E$ during growth phase, the total cross-tail E current increases by 1.3×10^6 A. Flow of this additional current through a 50-kV cross-tail potential difference generates an additional 60 GW of power, or a total additional energy of 1×10^{14} J in a 30-min growth phase. This is approximately equal to the total energy injected during a substorm [Stern, 1980].

Growth phase is associated with the southward turning of the interplanetary magnetic field (IMF). One effect of this IMF change is that magnetic field merging on the dayside may be enhanced. Since merging involves energy transfer, it often is assumed that the energy needed for a growth phase enters the magnetosphere in the dayside merging region. An alternate explanation associates growth phase energy input directly with an enhanced dawn to dusk cross-tail electric field. The interplanetary electric field (IEF) associated with solar wind flow is dusk to dawn as observed in the magnetospheric reference frame when the IMF is northward, and the IEF is dawn to dusk when the IMF is southward. Penetration of a portion of this IEF into the magnetosphere would enhance the plasma sheet dawn to dusk electric field during growth phase. Flow of cross-tail current through the enhanced cross-tail electric field could represent a significant growth phase energy source.

Current Diversion

It was found that dipolar field lines can exist very close to tail-like field lines if current is disrupted only in a wedge near midnight. Two satellites at synchronous altitude only a few earth radii apart see very different effects if one is inside the wedge and the other is not. It appears to be common to find wedges that expand suddenly either in the east-west direction or in radial extent during substorms. As a result, particle fluxes often increase in steps during a substorm [Arnoldy and Moore, 1983; Smits et al., 1986].

Current continuity must be maintained for each species or group of particles. Even though much of the cross-tail current is carried by ions, the diversion of electron current alone is sufficient to initiate tail collapse. One mechanism that can start this process is the onset of strong pitch angle scattering. Such scattering will fill the particle loss cones and therefore couples the magnetospheric plasma to the ionosphere. Once scattering has established a full loss cone, electron precipitation will form auroras, produce riometer absorption, and change ionospheric conductivities. These changes, plus the direct addition of diverted cross-tail currents, enhance electrojets and produce the well-known substorm features such as magnetic bays and AE index increases.

Acknowledgments. G. Ladreyt, D. Larson, K. Tang, and J. Lukas all contributed to the development of the magnetosphere model used throughout this report. R. L. Arnoldy made a number of very helpful suggestions with regard to particle fluxes and magnetic field changes near synchronous altitude. This work was supported by the National Science Foundation under grants ATM-84-00784 and ATM-85-21819.

The Editor thanks W. P. Olson and another referee for their assistance in evaluating this paper.

References

- Aggson, T. L., J. P. Heppner, and N.C. Maynard, Observations of large magnetospheric electric fields during the onset phase of a substorm, *J. Geophys. Res.*, **88**, 3981-3990, 1983.
- Arnoldy, R. L., and T. E. Moore, Longitudinal structure of substorm injections at synchronous orbit, *J. Geophys. Res.*, **88**, 6213-6220, 1983.
- Atkinson, G., The role of currents in plasma redistribution, in *Magnetospheric Currents*, *Geophys. Monogr. Ser.*, vol. 28, edited by T. A. Potemra, pp. 325-330, AGU, Washington, D. C., 1983.
- Baker, D. N., Particle and field signatures of substorms in the near magnetotail, in *Magnetic Reconnection in Space and Laboratory Plasmas*, *Geophys. Monogr. Ser.*, vol. 30, edited by E. W. Hones, Jr., pp. 193-202, AGU, Washington, D. C., 1984.
- Baker, D. N., E. W. Hones, Jr., P. R. Higbie, R. D. Belian, and P. Stauning, Global properties of the magnetosphere during a substorm growth phase: A case study, *J. Geophys. Res.*, **86**, 8941-8956, 1981.
- Beard, D. B., The magnetotail magnetic field, *J. Geophys. Res.*, **84**, 2118-2122, 1979.
- Beard, D. B., D. Hirschi, and K. Propp, The tailward magnetopause field beyond $10 R_E$, *J. Geophys. Res.*, **87**, 2533-2537, 1982.
- Bryant, D. A., Rocket studies of particle structure associated with auroral arcs, in *Physics of Auroral Arc Formation*, *Geophys. Monogr. Ser.*, vol. 25, edited by S.-I. Akasofu and J. R. Kan, pp. 103-111, AGU, Washington, D. C., 1981.
- DeForest, S. E., and C. E. McIlwain, Plasma clouds in the magnetosphere, *J. Geophys. Res.*, **76**, 3587-3611, 1971.

- Fairfield, D. H., Magnetotail energy storage and the variability of the magnetotail current sheet, in Magnetic Reconnection in Space and Laboratory Plasmas, Geophys. Monogr. Ser., vol. 30, edited by E. W. Hones, Jr., pp. 168-177, AGU, Washington, D. C., 1984.
- Fennell, J. F., D. R. Croley, and S. M. Kaye, Low-energy ion pitch angle distributions in the outer magnetosphere: Ion zipper distributions, J. Geophys. Res., 86, 3375-3382, 1981.
- Gray, P. C., and L. C. Lee, Particle pitch angle diffusion due to nonadiabatic effects in the plasma sheet, J. Geophys. Res., 87, 7445-7452, 1982.
- Hones, E. W., Jr., Plasma sheet behavior during substorms, in Magnetic Reconnection in Space and Laboratory Plasmas, Geophys. Monogr. Ser., vol. 30, edited by E. W. Hones, Jr., pp. 178-184, AGU, Washington, D. C., 1984.
- Kaufmann, R. L., Experimental tests for the acceleration of trapped particles, J. Geophys. Res., 68, 371-386, 1963.
- Kaufmann, R. L., What auroral electron and ion beams tell us about magnetosphere-ionosphere coupling, Space Sci. Rev., 37, 313-397, 1984.
- Kivelson, M. G., S. M. Kaye, and D. J. Southwood, The physics of plasma injection events, in Dynamics of the Magnetosphere, edited by S.-I. Akasofu, pp. 385-405, D. Reidel, Hingham, Mass., 1980.
- Kokubun, S., and R. L. McPherron, Substorm signatures at synchronous altitude, J. Geophys. Res., 86, 11265-11277, 1981.
- Lui, A. T. Y., Estimates of current changes in the geomagnetotail associated with a substorm, Geophys. Res. Lett., 5, 853-856, 1978.
- Mauk, B. H., and C.-I. Meng, Characterization of geostationary particle signatures based on the "injection boundary" model, J. Geophys. Res., 88, 3055-3071, 1983.
- McIlwain, C. E., Cold plasma boundaries and auroral arcs, in Physics of Auroral Arc Formation, Geophys. Monogr. Ser., vol. 25, edited by S.-I. Akasofu and J. R. Kan, pp. 173-174, AGU, Washington, D. C., 1981.
- McPherron, R. L., Substorm related changes in the geomagnetic tail: The growth phase, Planet. Space Sci., 20, 1521-1539, 1972.
- Moore, T. E., R. L. Arnoldy, J. Feynman, and D. A. Hardy, Propagating substorm injection fronts, J. Geophys. Res., 86, 6713-6726, 1981.
- Mullen, E. G., and M. S. Gussenhoven, SCATHA environmental atlas, Rep. AFGL-TR-83-0002, Air Force Geophys. Lab., Bedford, Mass., 1983.
- Nagai, T., D. N. Baker and P. R. Higbie, Development of substorm activity in multiple-onset substorms at synchronous altitude, J. Geophys. Res., 88, 6994-7004, 1983.
- Nishida, A., and Y. Kamide, Magnetospheric processes preceding the onset of an isolated substorm: A case study of the March 31, 1978, substorm, J. Geophys. Res., 88, 7005-7014, 1983.
- Olsen, R. C., Equatorially trapped plasma populations, J. Geophys. Res., 86, 11235-11245, 1981.
- Olson, W. P., A model of the distributed magnetospheric currents, J. Geophys. Res., 79, 3731-3738, 1974.
- Paulikas, G. A., and J. B. Blake, Effects of the solar wind on magnetospheric dynamics: Energetic electrons at the synchronous orbit, in Quantitative Modeling of Magnetospheric Processes, Geophys. Monogr. Ser., vol. 21, edited by W. P. Olson, pp. 180-202, AGU, Washington, D. C., 1979.
- Propp, K., and D. B. Beard, Cross-tail ion drift in a realistic model magnetotail, J. Geophys. Res., 89, 11013-11017, 1984.
- Roederer, J. G., On the adiabatic motion of energetic particles in a model magnetosphere, J. Geophys. Res., 72, 981-992, 1967.
- Sauvaud, J.-A. and J. R. Winckler, Dynamics of plasma, energetic particles, and fields near synchronous orbit in the nighttime sector during magnetospheric substorms, J. Geophys. Res., 85, 2043-2056, 1980.
- Schild, M. A., and L. A. Frank, Electron observations between the inner edge of the plasma sheet and the plasmasphere, J. Geophys. Res., 75, 5401-5414, 1970.
- Smits, D. P., W. J. Hughes, C. A. Cattell, and C. T. Russell, Observations of field-aligned currents, waves, and electric fields at substorm onset, J. Geophys. Res., 91, 121-134, 1986.
- Speiser, T. W., Particle trajectories in model current sheets, 1, Analytical solutions, J. Geophys. Res., 70, 4219-4226, 1965.
- Speiser, T. W., Particle trajectories in model current sheets, 2, Applications to auroras using a geomagnetic tail model, J. Geophys. Res., 72, 3919-3932, 1967.
- Stern, D. P., Energetics of the magnetosphere, NASA Tech. Memo., 82039, 1-12, 1980.
- Stern, D. P., The magnetic field of the inner edge of the plasma sheet (abstract), Eos Trans. AGU, 67, 355, 1986.
- Tsyganenko, N. A., and A. V. Usmanov, Determination of the magnetospheric current system parameters and development of experimental geomagnetic field models based on data from IMP and HEOS satellites, Planet. Space Sci., 30, 985-998, 1982.
- Wagner, J. S., J. R. Kan, and S.-I. Akasofu, Particle dynamics in the plasma sheet, J. Geophys. Res., 84, 891-897, 1979.

R. L. Kaufmann, Department of Physics, DeMeritt Hall, University of New Hampshire, Durham, NH 03824.

(Received May 6, 1986;
revised March 2, 1987;
accepted February 27, 1987.)